American Mineralogist, Volume 75, pages 847–858, 1990

Layer topology, stacking variation, and site distortion in melilite-related compounds in the system CaO-ZnO-GeO_2-SiO_2

THOMAS ARMBRUSTER
Laboratorium für chemische und mineralogische Kristallographie, Universität Bern, Freiestrasse 3, CH-3012 Bern, Switzerland

FRANÇOIS RÖTHLISBERGER, FRIEDRICH SEIFERT
Bayerisches Forschungsinstitut für experimentelle Geochemie und Geophysik, Universität Bayreuth, Postfach 10 12 51, D-8580 Bayreuth, F.R.G.

ABSTRACT

Single crystals of melilite-related tetrahedral sheet structures in the system CaO-ZnO-GeO_2-SiO_2 were grown by hydrothermal methods, sinter experiments, flux, and topotactical techniques. Their crystal structures were determined and refined using X-ray single-crystal data.

The high-temperature polymorph, high-$Ca_2ZnGe_2O_7$, possesses an incommensurate structure at room temperature. The average structure with space group $P\bar{4}2_1m$, $a = 7.950(1)$, $c = 5.186(1)$ Å is of melilite type with layers formed by ZnO_4 and GeO_4 tetrahedra. Anisotropic displacement parameters indicate that the modulation may be interpreted in terms of librations of tetrahedral units about the c axis.

Low-$Ca_2ZnGe_2O_7$, grown from a Na_2WO_4 flux or by an epitaxial method, also possesses an incommensurate fine structure. The refined average structure, space group $P2_1$, $a = 8.020(2)$, $b = 7.995(2)$, $c = 15.506(3)$ Å, $\beta = 89.47(2)°$ displays a stacking variant of melilite-like layers with an ABA′ABA′ stacking sequence. The stacking fragment A′A is essentially a melilite unit. Layer B is rotated 90° about c relative to layer A. Ca atoms between layers A and B have a disordered arrangement.

A new tetrahedral sheet structure with four-, five-, and six-membered rings of tetrahedra was synthesized at the lowest temperatures. The structure has space group $P2_1/n$, $a = 9.112(1)$, $b = 7.900(2)$, $c = 9.380(1)$ Å, $\beta = 114.03(1)°$ and is well ordered without any indication of modulation.

INTRODUCTION

Melilite-type compounds of general stoichiometry $X_2T_3A_7$ (with X = large, monovalent to trivalent cation, T = small divalent to quadrivalent cation, A = anion) are widespread among sulfides, oxysulfides, oxides, and silicates, and the latter also form an important group of natural minerals. Their structure (e.g., Smith, 1953) can be described in space group $P\bar{4}2_1m$ and consists of T_2A_7 tetrahedral dimers (T2 sites) connected by means of additional tetrahedrally coordinated cations (T1 sites) to form tetrahedral sheets, with the large X cations in distorted eight-coordinated sites between the sheets (Fig. 1). Meliphanite, $Ca(Ca,Na)BeSi_2O_6F$ (Dal Negro et al., 1967) and leucophanite, $CaNaBeSi_2O_6F$ (Grice and Hawthorne, 1989) also possess a melilite-like structure. However, because of cation- and anion-(O,F) ordering, the symmetry is lowered to $I\bar{4}$ and $P2_12_12_1$, respectively.

It has been recognized by Hemingway et al. (1985) and Seifert et al. (1987) that $Ca_2MgSi_2O_7$ and solid solutions with component $Ca_2FeSi_2O_7$ undergo a reversible phase transition to a low-temperature incommensurate phase at ca. 358 to 523 K, depending on composition. Since those studies, this phase transition has been recognized to occur in all $Ca_2T1Si_2O_7$ melilites (with T1 = Mg,Zn, Fe,Co,Mn and mixtures thereof) but not in $Ca_2BeSi_2O_7$ (Röthlisberger, 1989). This is in line with the argument proposed independently by Hemingway et al. (1985) and Seifert et al. (1987) that the formation of the incommensurate melilite phase is due to a structural misfit between the dimensions of the tetrahedral sheet on the one hand and the size of the interlayer (X = Ca) cation on the other. Only at elevated temperatures does dynamic disorder of the X ions lead to a stabilization of the unmodulated melilite structure.

The theory for modulated phases predicts that they are intermediate between a commensurate high-temperature phase (in this case the unmodulated melilite structure) and a (commensurate) low-temperature superstructure. Except for $Ca_2CoSi_2O_7$, where such a superstructure might occur metastably in the vicinity of 77 K (Röthlisberger, 1989), no experimental proof of the existence of low-temperature superstructures of the melilite type has been obtained so far.

Based on the above concept, it was expected that max-

0003–004X/90/0708–0847$02.00

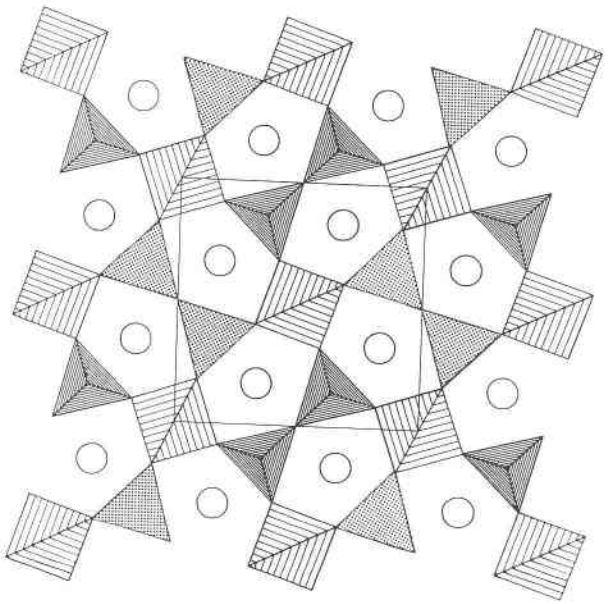

Fig. 1. Coordination polyhedron diagram of the melilite structure viewed along the *c* axis. In the average high-$Ca_2ZnGe_2O_7$ structure and the average $Ca_2ZnSi_2O_7$ structure, ZnO_4 (T1) tetrahedra are at 0,0,0 and ½,½,0 and connect Ge_2O_7 and Si_2O_7 groups (T2). Open circles represent Ca atoms at z = 0.5.

imizing the structural misfit by even further expansion of the dimensions of the tetrahedral sheet would lead to a stabilization of low-temperature structural variants of the melilite type. Therefore, we have replaced the Si in $Ca_2ZnSi_2O_7$ by larger Ge atoms and studied both the Ge end-member and a phase with intermediate composition. A second reason for the selection of the system CaO-ZnO-GeO_2-SiO_2 as an example of melilite-related structures is the specific crystal-chemical behavior of Zn and Ge in oxides. At temperatures below 970 K akermanite $Ca_2MgSi_2O_7$ decomposes into a chain silicate (wollastonite) and a nesosilicate structure (monticellite); thus stable low-temperature melilite-type compounds cannot be expected in this system. In contrast, Zn prefers tetrahedral coordination and Ge^{4+} tends to form extended polyanions to a much smaller degree than Si.

Experimental procedure

Crystal growth

High $Ca_2ZnGe_2O_7$. Stoichiometric mixtures of analysis-grade $CaCO_3$, ZnO, and GeO_2 were slowly (8 K/min) heated to 1373 K, in order to decarbonize the mixtures. The reground powder was placed in a Pt crucible and slowly heated until the sample melted. For 15 minutes the melting point (1483–1493 K) was exceeded by 20 to 30 K. The temperature was then continuously lowered (3 K/min) to 1463 K, where all $Ca_2ZnGe_2O_7$ had crystallized. After quenching the crucible onto a steel plate, it was immersed in water. The sample contained colorless, transparent, platy crystals up to 1 mm in diameter.

Low $Ca_2ZnGe_2O_7$. Two methods were used. For epitaxial growth, the outer portions of the high $Ca_2ZnGe_2O_7$ sample were partly melted in a Pt crucible and then quenched as above. At this point the sample consisted of a high-$Ca_2ZnGe_2O_7$ core with a glass rim. The glass was subsequently recrystallized by slow continuous heating from 1023 K to 1273 K and maintained 12 h at the final temperature. Crystals up to 0.5 mm in diameter formed aggregates on the rim. The original high phase in the core acted as a nucleus and turned milky white, probably indicating that a phase transition had occurred.

Crystals were also successfully grown in a disodium tungstate flux (dehydrated $Na_2WO_4 \cdot 2H_2O$). This melt is soluble in water, which promotes separation of the crystals. The starting material was a powder of composition $Ca_2ZnGe_2O_7$, which was mixed with the flux in an approximate ratio of 1:10. The mixture was continuously (8 K/min) heated in a Pt crucible to 1293 K until the melt was homogeneous. Subsequently, additional $Ca_2ZnGe_2O_7$ was added until no more dissolved; the temperature was raised by 50 K until all aggregates had disappeared and maintained constant for 30 min; then the temperature was lowered (between 1 and 3 K/h) to 1023 K. This method yielded platy crystals up to 3 mm in their maximum dimension. Often the crystals were twinned or milky white.

$Ca_2ZnGe_{1.25}Si_{0.75}O_7$. Single crystals of this compound were synthesized from high-purity grade $Ca(OH)_2$, ZnO, SiO_2, and GeO_2 in the molar proportions 2:1:1:1. Homogenized mixtures were dried at 353 K and used as starting material for hydrothermal syntheses. The samples were placed in a small Au capsule with 30% NaOH solution as solvent and sealed. Conventional hydrothermal pressure vessels were used for 34 days at 828 K and 2 kbar. The platy experimental products consisted of the monoclinic phase $Ca_2ZnGe_{1.25}Si_{0.75}O_7$ (composition from crystal-structure site-occupancy refinements) and Si-rich melilite. This monoclinic phase could also be grown as the pure Ge end-member. Hydrothermal experiments conducted for 17 d at 890 K and 6200 bars with only $Ca(OH)_2$, ZnO, and GeO_2 (2:1:2) and H_2O yielded an X-ray powder pattern (Guinier camera Cu$K\alpha_1$-radiation) corresponding to that of the compound $Ca_2ZnGe_{1.25}Si_{0.75}O_7$. The same pattern was obtained when a melilite-type powder sample with the composition $Ca_2ZnGe_2O_7$ was sintered at 1345 K or 1270 K. Unfortunately, suitable single crystals of this end-member phase were not found in either batch. Thus the structure was refined for the (Ge,Si) solid-solution member.

Crystal-structure analysis

Several crystals of each type were studied using a precession camera (Mo$K\alpha$ X-radiation) for space-group determination and crystal quality control. These investigations indicated that both low and high $Ca_2ZnGe_2O_7$ exhibit incommensurate satellite reflections owing to a modulation within the (001) layers. These satellites are much stronger for high $Ca_2ZnGe_2O_7$ than for low

TABLE 1. Cell dimensions and experimental data

Compound	Average high $CaZnGe_2O_7$ tetragonal	Average low $CaZnGe_2O_7$ monoclinic	$Ca_2ZnGe_{1.25}Si_{0.75}O_7$ monoclinic
Space group	$P\bar{4}2_1m$	$P2_1$	$P2_1/n$
a (Å)	7.950(1)	8.020(2)	9.112(1)
b (Å)	7.950(1)	7.995(2)	7.900(2)
c (Å)	5.186(1)	15.506(3)	9.380(1)
α (°)	90	90	90
β (°)	90	89.47(2)	114.03(1)
γ (°)	90	90	90
θ-limit (°)	40	30	30
No. Refl.	635	2422	1680
No. Obs. $>6\sigma(F_{obs})$	560	2334	1420
No. param.	34	351	101
R_w (%)	7.2	3.41	2.47
R (%)	5.4	2.97	1.68

Note: $R = \Sigma||F_{obs}| - |F_{calc}||/\Sigma|F_{obs}|$,
$R_w = (\Sigma w(|F_{obs}| - |F_{calc}|)^2/\Sigma w|F_{obs}|^2)^{1/2}$.

$Ca_2ZnGe_2O_7$, where the additional reflections can only be observed in strongly overexposed photographs. The aim of the present study is a determination and discussion of the average structures, whereas an analysis of the modulation will be left for a forthcoming study. $Ca_2ZnGe_{1.25}Si_{0.75}O_7$ gave sharp reflections without any satellites.

All reflection intensities were measured at room temperature in the ω-scan mode using graphite monochromatized Mo$K\alpha$ radiation and a CAD4 Enraf Nonius diffractometer. Additional data pertaining to experimental conditions are summarized in Table 1. Empirical absorption corrections were applied to all crystals using the ψ-scan technique. Data reduction, including background and Lorentz-polarization corrections, was carried out with the SDP program system (Enraf Nonius, 1983). The structures of low $Ca_2ZnGe_2O_7$ and $Ca_2ZnGe_{1.25}Si_{0.75}O_7$ were solved by direct methods and subsequent Fourier analyses using the program SHELXS-86 (Sheldrick, 1986). The program SHELX76 (Sheldrick, 1976) was applied for structure refinement. Because space group, cell size, and powder data obtained for high $Ca_2ZnGe_2O_7$ indicated its structure to be of the well-known melilite type, structure refinement was initiated with the structure parameters of $Ca_2ZnSi_2O_7$ (Louisnathan, 1969) and the program Prometheus (Zucker et al., 1983). Neutral-atom scattering factors and real as well as imaginary anomalous dispersion corrections were applied. Structure factors with a cutoff $F_{obs} > 6\ \sigma\ (F_{obs})$ were weighted with the value $1/\sigma^2$. In the case of low-$Ca_2ZnGe_2O_7$, the average structure was refined with unit weights because it was not clear whether reflection intensities were influenced by neighboring satellites.

RESULTS

Average high-$Ca_2ZnGe_2O_7$ structure

Observed and calculated structure factors are summarized in Table 2.[1] Final atomic coordinates and displacement parameters are given in Table 3. The strong anisotropy of several displacement parameters (Fig. 2) reflects the modulation within (001). It is evident that the major effect of the modulation is a coupled libration of the tetrahedra around **c** combined with a translation of Ca along ⟨110⟩. When the average structure of high $Ca_2ZnGe_2O_7$ is compared with the structure of natural $Ca_2ZnSi_2O_7$ (Louisnathan, 1969), the orientation of the probability displacement ellipsoids is seen to be very similar, though less pronounced in the silicate (Fig. 2). Recent electron microscopic investigations (Röthlisberger, 1989) on material from the same type locality indicated that natural $Ca_2ZnSi_2O_7$ (hardystonite) also exhibits incommensurate superstructure reflections. The Zn-O bond distance in the Ge compound is 1.95 Å, and the Ge-O distances vary between 1.68 and 1.74 Å. The mean Ca-O distance for eight-coordinated Ca is 2.60 Å. Corresponding distances in the silicate are Zn-O = 1.937 Å, ⟨Si-O⟩ = 1.618 Å, and ⟨Ca-O⟩ = 2.569 Å (Louisnathan, 1969). Selected individual interatomic distances and angles are given in Table 4.

Average low-$Ca_2ZnGe_2O_7$ structure

The structure of this compound is a new melilite-related structure with a stacking sequence of tetrahedral

[1] To obtain copies of Tables 2, 5, and 9, order Document AM-90-434 from the Business Office, Mineralogical Society of America, 1130 Seventeenth Street NW, Suite 330, Washington, DC 20036, USA. Please remit $5.00 in advance for the microfiche.

TABLE 3. Atom coordinates and displacement parameters U_{ij} (Å²) for the average high-$Ca_2ZnGe_2O_7$ structure

Atom	Ca X	Zn T1	Ge T2	O1	O2	O3
x	0.3320(2)	0	0.14206(9)	0.5	0.1400(8)	0.088(2)
y	0.1680	0	0.35794	0	0.3600	0.179(1)
z	0.5038(6)	0	0.9531(2)	0.181(3)	0.277(2)	0.783(2)
B_{eq} (Å²)	2.96(3)	1.27(1)	1.08(1)	6.1(4)	2.5(1)	7.3(4)
U_{11}	0.049(1)	0.0196(4)	0.0152(2)	0.11(2)	0.042(3)	0.20(1)
U_{22}	0.049	0.0196	0.0152	0.11	0.042	0.042(4)
U_{33}	0.0141(8)	0.0092(6)	0.0109(4)	0.006(4)	0.012(3)	0.031(4)
U_{12}	0.038(1)	0	0.0002(3)	−0.09(2)	0.025(5)	−0.075(7)
U_{13}	0.0001(5)	0	0.0040(2)	0	−0.002(2)	0.061(6)
U_{23}	−0.0001	0	−0.0040	0	0.002	−0.026(4)

Note: $B_{eq} = 8/3\ \pi^2\ \Sigma_i(\Sigma_j(U_{ij}\ a_i^*\ a_j^*\ a_i \cdot a_j))$, $\sigma(B_{eq})$: Schomaker and Marsh (1983), displacement parameters are of the form: $\exp[-2\pi^2(U_{11}h^2a^{*2} + U_{22}k^2b^{*2} + U_{33}l^2c^{*2} + 2U_{12}hka^*b^* + 2U_{13}hla^*c^* + 2U_{23}klb^*c^*)]$.

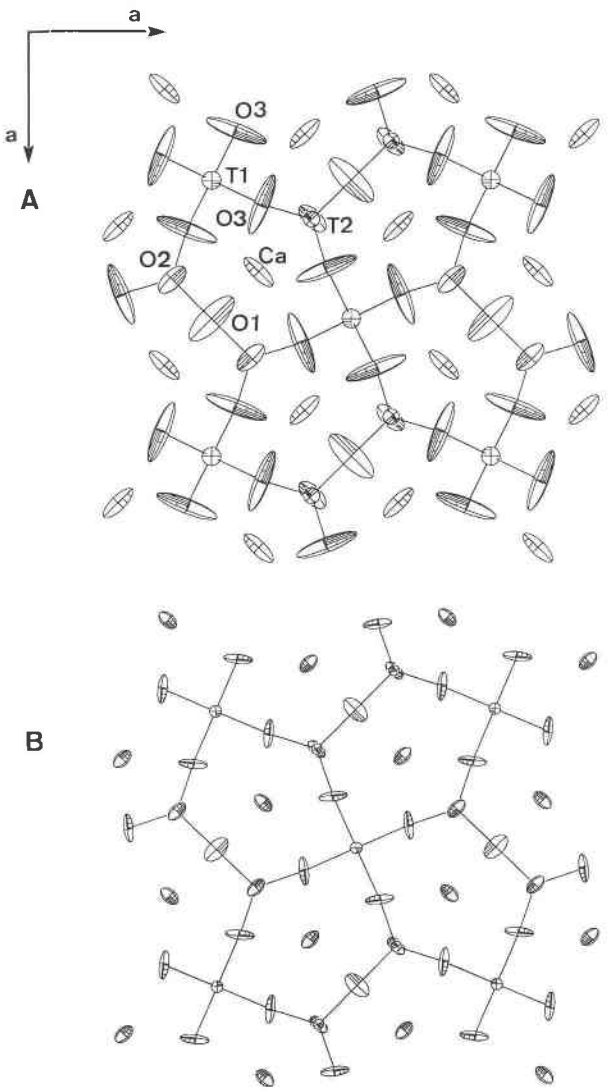

Fig. 2. ORTEP plots of melilite-type structures viewed along the *c* axis. (**A**) average high-$Ca_2ZnGe_2O_7$ structure: note the strong anisotropy of selected O and Ca displacement ellipsoids. The resulting pattern can be interpreted in terms of rotations of tetrahedral units parallel to the *c* axis. (**B**) average $Ca_2ZnSi_2O_7$: the orientation of the displacement ellipsoids is similar to A, but the anisotropy and size of the ellipsoids are less pronounced. This observation is in agreement with the fact that $Ca_2ZnSi_2O_7$ also exhibits incommensurate superstructure reflections. (Scale of displacement ellipsoids is 70%.)

layers different and more complex (Fig. 3) than that of melilite. Whereas in melilite the layers are stacked directly one above the other (AA sequence, period $c = 5.188$ Å), in average low $Ca_2ZnGe_2O_7$ the *c* axis is tripled (15.506 Å), reflecting the stacking sequence ABA′ABA′ (Fig. 4). The melilite-related layers A and A′ are identical, as they can be derived from each other by a 2_1 (along *b*) axis. The A′A fragment of the structure represents a melilite-type unit. Layer B also displays the characteristic features of a melilite-type layer (five-membered rings of tetrahedra). However, it is rotated by 90° around the *c* axis with respect to layer A or A′ and also slightly shifted along **a** (Fig. 4).

Table 4. Selected interatomic distances (Å) for melilite-type average $Ca_2ZnGe_2O_7$ and $Ca_2ZnSi_2O_7$ structures

	$Ca_2ZnGe_2O_7$	$Ca_2ZnSi_2O_7$
Ca-O1	2.52(1)	2.484(5)
Ca-O2	2.457(6)	2.472(4)
Ca-O3*	2.42(2)	2.412(4)
Ca-O2′*	2.708(4)	2.699(4)
Ca-O3′*	2.80(1)	2.685(4)
Zn-O3	1.95(1)	1.937(4)
T2-O3*	1.73(1)	1.619(4)
T2-O2	1.68(1)	1.583(5)
T2-O1	1.742(6)	1.649(3)
T2-O1-T2	133(1)	138.5(5)
Zn-O3-T2	113.5(5)	117.33(3)

Note: Distances marked * occur twice.

A stack of layers ABA′ yields two channel systems parallel to **c**. There are channels (type 1) formed by five-membered rings of tetrahedra of different orientation stacked above each other. A second, more irregular channel type, (type 2) is formed by superimposed five-membered rings that overlap only in a narrow square (Fig. 3). Ca in type-1 channels occupies the intermediate layers at $z = 0$, $\frac{1}{3}$, $\frac{2}{3}$, as in melilite. Ca in type-2 channels is also located on these intermediate layers but in a disordered manner. Difference-Fourier maps yielded three strong residual peaks for the two available Ca atoms. Two of these peaks were highly asymmetric and could not be modeled by conventional anisotropic displacement parameters. They were modeled by split half-atoms. In the final refinement Ca population factors for type-2 channel sites were allowed to vary. Unconstrained occupancy refinements yielded a total of 6.25(25) Ca, which is in good agreement (1 σ) with the 6.0 Ca required by the formula. The disordered Ca atoms affect the positions of the O atoms coordinating Ca, as evident from the anisotropy of O displacement parameters. However, a split-oxygen model was not used because of obvious correlation problems. Such correlations required that U_{33} parameters of selected O atoms had to be fixed to obtain positive-definite displacement matrices for all O atoms. The observed disorder effects are probably related to the modulated character of the fine structure. Observed and calculated structure factors are summarized in Table 5 (see footnote 1). Final coordinates, anisotropic displacement parameters, and interatomic distances are given in Tables 6, 7, and 8, respectively.

The following nomenclature is used for atomic positions: The layer type A or B is indicated by subscripts. In addition, cations and anions are arbitrarily numbered. Ca on the intermediate layer with $z = 0$ is indicated by Ca_a, and Ca on the layers with $z \sim \frac{1}{3}$, $\frac{2}{3}$ is indicated by

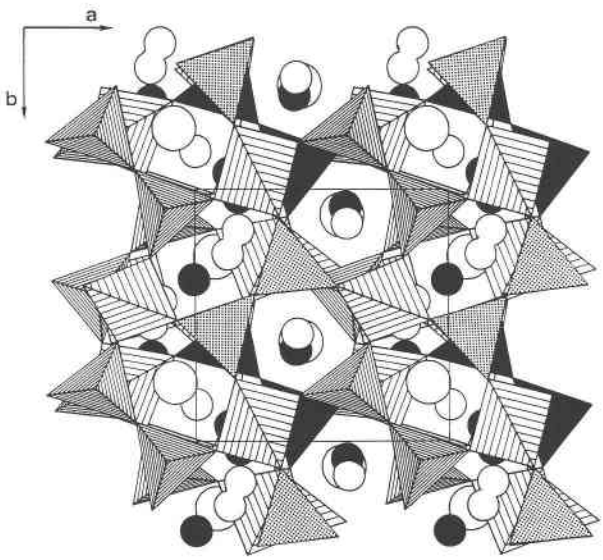

Fig. 3. Coordination polyhedron diagram of the average low-$Ca_2ZnGe_2O_7$ structure viewed along the *c* axis. Melilite-type layers are stacked in an ABA'ABA' sequence. Large open circles represent Ca atoms at $z \approx 0, 1$, filled small circles Ca atoms at $z \approx 1/3$, and open small circles Ca atoms at $z \approx 2/3$. The peanut-shaped overlapping circles are due to split Ca atoms with the same z coordinate. For a more detailed description of the structure consult the text.

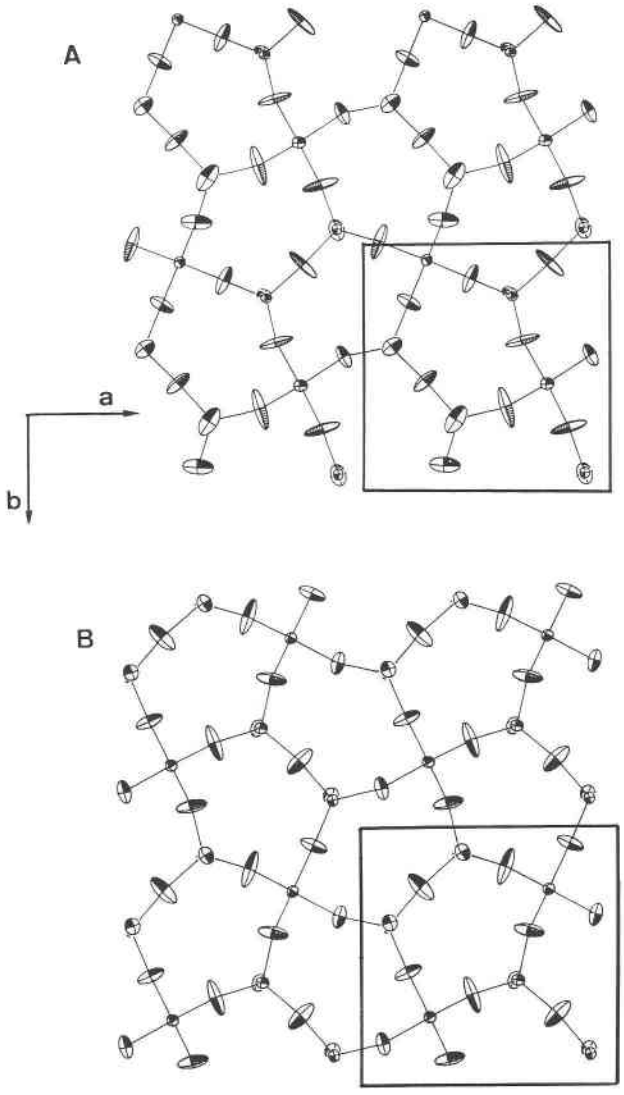

Fig. 4. ORTEP plot of the average low-$Ca_2ZnGe_2O_7$ structure viewed along the *c* axis. Note the strong anisotropy of displacement ellipsoids, which is caused by the incommensurate fine structure. (**A**) layer type A at $z \approx 1/6$; (**B**) layer type B at $z \approx 1/2$. (Scale of displacement ellipsoids is 50%.)

Ca_b. Eight-coordinated Ca_a1 and Ca_a2 positioned between A and A' layers yield ⟨Ca-O⟩ distances of 2.60 and 2.62 Å, respectively. These values are almost identical to those in high $Ca_2ZnGe_2O_7$. Ca_b1 and Ca_b2 are positioned in a type-1 channel. Ca_b1 is also eight-coordinated (⟨Ca-O⟩ = 2.59), and Ca_b2 is seven-coordinated (⟨Ca-O⟩ = 2.58 Å). Ca_b3, in a type-2 channel, is only occupied to 61% and has six O neighbors with distorted octahedral coordination (⟨Ca-O⟩ = 2.52 Å). The remaining disordered Ca atoms Ca_b4a, Ca_b4b, Ca_b5a, and Ca_b5b in the type-2 channel have between five and seven O neighbors with distances between 2.1 and 3.2 Å. The anisotropy of probability displacement ellipsoids (Table 7) indicates that the disorder within the tetrahedral layers may be best described by librations of individual tetrahedra around the *c* axis. Displacement parameters of atoms on the libration axis yield displacement ellipsoids that are approximately isotropic. As in high $Ca_2ZnGe_2O_7$, Ca ellipsoids are elongated along ⟨110⟩. For split Ca positions this anisitropy is defined by the orientation of the Ca_b4a-Ca_b4b and Ca_b5a-Ca_b5b vectors.

$P2_1/n$ $Ca_2ZnGe_{1.25}Si_{0.75}O_7$ structure

This compound is the only one of the three studied structures that crystallizes with a centric space group. The orientation of crystal axes is also different from that of the other two structures. Observed and calculated structure factors are summarized in Table 9 (see footnote 1). Atomic coordinates are listed in Table 10 and anisotropic displacement parameters are in Table 11. Selected interatomic distances are given in Table 12. The tetrahedral layers are parallel to (101), and the stacking is along [101] (stacking period 10 Å). The tetrahedral layers (Fig. 5) are different than those of melilite, as the tetrahedra not only form five-membered rings but also occur in four- and strongly distorted six-membered units (Fig. 6). Site population refinements with Ge and Si form factors for the tetrahedral atoms Ge2 and Ge3 indicate a partly ordered (Ge,Si) distribution. The Ge2 position is occupied by 73% Ge and 27% Si, whereas the Ge3 site is occupied by 52% Ge and 48% Si. This difference is also reflected in mean

TABLE 6. Population factors, coordinates, and equivalent isotropic displacement factors for the average low-$Ca_2ZnGe_2O_7$ structure

Atom	Pop.	x	y	z	B_{eq} (Å²)
Zn_A1	1.0	−0.2615(2)	−0.0646(2)	0.1543(1)	1.11(2)
Zn_A2	1.0	−0.7447(2)	0.4237(2)	0.1646(1)	1.28(2)
Ge_A3	1.0	−0.6072(2)	0.7837(3)	0.1464(1)	0.85(2)
Ge_A4	1.0	−0.3880(2)	0.2840(3)	0.1913(1)	1.38(2)
Ge_A5	1.0	−0.1131(2)	0.5788(3)	0.1836(1)	1.07(2)
Ge_A6	1.0	−0.8972(2)	0.0643(3)	0.1508(1)	0.87(2)
Zn_B1	1.0	−0.7332(2)	0.7644(2)	0.5085(1)	1.10(2)
Ge_B2	1.0	−0.6125(2)	0.4077(3)	0.4721(1)	1.04(2)
Ge_B3	1.0	−0.1070(2)	0.6183(3)	0.5169(1)	0.86(2)
Ca_a1	1.0	0.4168(6)	0.0996(6)	0.0004(2)	2.85(8)
Ca_a2	1.0	0.0814(5)	0.7646(6)	−0.0052(2)	3.10(7)
Ca_b1	1.0	0.4042(5)	0.0684(5)	0.3308(2)	1.82(5)
Ca_b2	1.0	0.6011(4)	0.6316(6)	0.3373(2)	2.00(6)
Ca_b3	0.61(1)	−0.002(2)	0.346(2)	0.3297(7)	5.9(2)
Ca_b4a	0.37(5)	0.125(2)	−0.243(1)	0.3254(7)	1.4(2)
Ca_b4b	0.41(6)	0.172(4)	0.696(8)	0.331(1)	7.2(8)
Ca_b5a	0.52(6)	0.866(2)	0.936(1)	0.3437(7)	1.9(2)
Ca_b5b	0.35(7)	0.834(6)	0.01(1)	0.332(2)	8.2(2)
O_A1	1.0	0.562(2)	0.858(2)	0.0848(7)	3.3(3)
O_A2	1.0	0.104(2)	0.061(2)	0.2612(6)	2.1(2)
O_A3	1.0	0.077(1)	−0.459(2)	0.2297(6)	2.4(2)
O_A4	1.0	0.241(2)	−0.080(3)	0.1034(8)	4.8(4)
O_A5	1.0	0.353(3)	0.602(2)	0.096(1)	4.6(5)
O_A6	1.0	0.401(1)	−0.203(2)	0.2578(6)	1.5(2)
O_A7	1.0	0.420(2)	0.329(3)	0.2393(9)	6.2(6)
O_A8	1.0	0.168(2)	0.247(2)	0.0980(8)	5.0(4)
O_A9	1.0	0.811(2)	0.762(2)	0.2343(7)	2.8(3)
O_A10	1.0	0.748(2)	0.438(2)	0.2338(7)	3.2(2)
O_A11	1.0	0.670(3)	0.100(2)	0.2435(9)	4.0(4)
O_A12	1.0	0.624(2)	0.281(2)	0.0802(7)	3.8(3)
O_A13	1.0	0.881(2)	0.581(2)	0.0719(8)	2.5(2)
O_A14	1.0	0.931(2)	0.012(3)	0.0906(8)	5.1(5)
O_B1	1.0	0.113(2)	0.136(2)	0.5934(7)	1.8(2)
O_B2	1.0	−0.399(1)	−0.092(2)	0.4157(6)	1.7(2)
O_B3	1.0	0.183(2)	−0.060(2)	0.4316(7)	2.8(3)
O_B4	1.0	0.344(2)	−0.398(2)	0.423(1)	3.6(4)
O_B5	1.0	0.235(2)	0.274(2)	0.4315(8)	4.1(3)
O_B6	1.0	−0.084(2)	0.162(2)	0.4345(7)	2.2(2)
O_B7	1.0	0.567(2)	0.352(3)	0.4174(8)	4.5(5)

Note: $B_{eq} = 8/3\ \pi^2\ \Sigma_i(\Sigma_j(U_{ij}\ a_i^*\ a_j^*\ a_i \cdot a_j))$, standard deviations in parentheses, $\sigma(B_{eq})$: Schomaker and Marsh (1983).

T-O distances (⟨T-O⟩), which are 1.7208 Å for Ge2 and 1.6943 Å for Ge3. The layers are stacked in an ABAB sequence, where the sheets A and B are symmetrically equivalent but shifted along [$\bar{1}$01]/2 with respect to each other. The tetrahedral sheet structure is characterized by two channel types running parallel to [101]. As in low $Ca_2ZnGe_2O_7$, the first channel type is formed by the stacking of five-membered rings of tetrahedra that are rotated relative to one another (Fig. 5). Ca occupying this kind of channel is eight-coordinated (square antiprism) with ⟨Ca-O⟩ = 2.569 Å. The second narrow channel type is formed by an alternating sequence along [101] of four-membered and elongated six-membered rings. Ca between the rings is in distorted octahedral coordination with ⟨Ca-O⟩ = 2.419. Also striking is the small Ge2-O-Ge3 angle of 122°. In addition, the tetrahedra display strongly irregular T-O distances (Ge2: 1.658–1.729 Å). The largest distance is observed for the bridging O atom of Ge2-O-Ge3. Ca is well ordered.

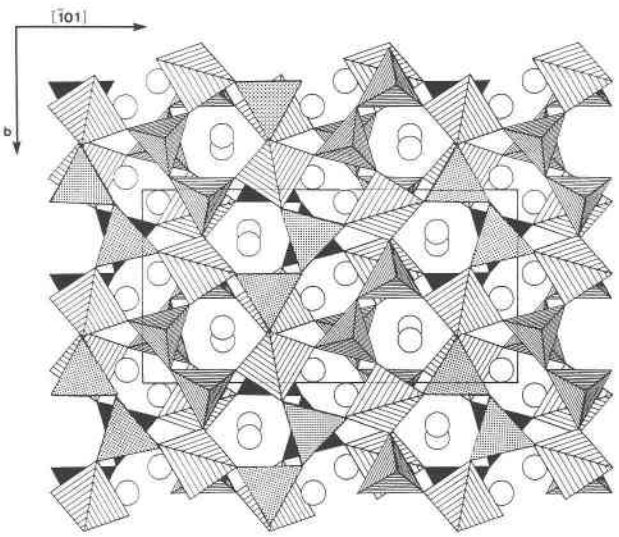

Fig. 5. Coordination polyhedron diagram of the structure of $Ca_2ZnGe_{1.25}Si_{0.75}O_7$ (space group $P2_1/n$). The structure is viewed parallel to [101], perpendicular to the tetrahedral layers. The layers (101) are stacked in an ABAB sequence. Pairs of tetrahedra with vertices pointing up or down are occupied by Ge and Si, distorted tetrahedra seen edgewise are occupied by Zn. Open circles represent Ca. Three types of tetrahedral rings are present: five-membered rings, four-membered rings, and extremely elongated six-membered units.

DISCUSSION

Layer topology

Tetrahedral layer structures that do not occur in ordinary sheet silicates are composed of vertex-sharing tetrahedra centered by Be, P, Si, B, Al, Mg, Fe, Co, Zn, etc. These tetrahedral sheets are primarily linked by "soft cations" like Na, K, Ca, Sr, and Ba (Liebau, 1985) that have no pronounced preference for one or another kind of well-defined coordination polyhedron. In contrast to tetrahedral sheets in micas, the sheets discussed here have two identical surfaces, with large cations both above and below.

The topology of tetrahedral sheets can be described with Schläfli symbols (Liebau, 1985), where each tetrahedron is represented by a point and the resulting points are connected to form a network of polygons (Fig. 7). Each polygon is specified by the number of corners. A node of the network is described by its surrounding polygons. Superscripts denote the number of equal polygons neighboring the node. A network is described by listing the nodes with nonequivalent polygon surroundings and indicating the relative frequency of such nodes by right subscripts.

According to this nomenclature, a melilite-type layer with five-membered tetrahedral rings has the symbol (5^4) $(5^3)_2$. A review of compounds with the melilite structure type is given by Bakakin et al. (1970) and Röthlisberger (1989). The structure of $P2_1/n$ Ca_2 $(Ge,Si)_2O_7$ described in this paper possesses four-, five-, and six-membered

TABLE 7. Displacement parameters U_{ij} (Å^2) for the average low-$Ca_2ZnGe_2O_7$ structure

Atom	U_{11}	U_{22}	U_{33}	U_{12}	U_{13}	U_{23}
Zn_A1	0.0147(7)	0.0153(7)	0.0123(6)	−0.0005(6)	0.0018(5)	0.0020(6)
Zn_A2	0.0212(7)	0.0153(7)	0.0122(6)	0.0001(6)	0.0023(5)	−0.0007(6)
Ge_A3	0.0145(6)	0.0097(5)	0.0081(5)	0.0001(5)	0.0019(4)	−0.0019(5)
Ge_A4	0.0197(7)	0.0223(7)	0.0103(5)	−0.0016(6)	0.0047(5)	−0.0021(6)
Ge_A5	0.0205(8)	0.0150(7)	0.0052(5)	0.0017(5)	0.0011(5)	−0.0013(5)
Ge_A6	0.0119(6)	0.0141(6)	0.0071(5)	0.0001(6)	−0.0003(5)	0.0005(5)
Zn_B1	0.0153(7)	0.0145(7)	0.0121(6)	−0.0005(6)	0.0024(5)	0.0022(6)
Ge_B2	0.0178(7)	0.0129(7)	0.0088(5)	0.0012(6)	0.0034(5)	0.0003(5)
Ge_B3	0.0128(7)	0.0146(7)	0.0052(6)	−0.0005(5)	−0.0008(5)	−0.0002(5)
Ca_a1	0.041(2)	0.055(3)	0.012(1)	−0.031(2)	0.000(1)	0.009(1)
Ca_a2	0.047(2)	0.058(2)	0.013(1)	−0.037(2)	0.002(1)	−0.006(1)
Ca_b1	0.031(2)	0.026(1)	0.012(1)	0.012(2)	0.012(1)	0.007(1)
Ca_b2	0.026(2)	0.034(2)	0.015(1)	0.017(2)	0.010(1)	0.013(1)
Ca_b3	0.091(6)	0.087(6)	0.047(4)	0.039(4)	0.023(4)	0.043(4)
Ca_b4a	0.027(6)	0.022(7)	0.006(4)	−0.015(4)	0.008(3)	−0.002(3)
Ca_b4b	0.06(1)	0.18(3)	0.041(8)	−0.01(2)	−0.007(8)	−0.03(1)
Ca_b5a	0.035(6)	0.027(6)	0.009(4)	−0.003(4)	0.005(3)	−0.004(3)
Ca_b5b	0.11(2)	0.17(5)	0.03(1)	−0.05(3)	0.01(1)	−0.02(2)
O_A1	0.030(6)	0.09(1)	0.009(5)	−0.033(7)	0.004(4)	−0.006(5)
O_A2	0.029(6)	0.049(7)	0.001(3)	0.008(6)	0.000(4)	−0.002(5)
O_A3	0.027(6)	0.054(8)	0.009(4)	0.021(6)	0.002(4)	−0.005(5)
O_A4	0.09(1)	0.08(1)	0.01510*	0.07(1)	−0.004(6)	−0.012(7)
O_A5	0.13(2)	0.018(7)	0.029(8)	−0.034(8)	0.04(1)	−0.012(5)
O_A6	0.028(5)	0.017(5)	0.011(4)	0.006(4)	−0.001(4)	0.002(4)
O_A7	0.030(7)	0.18(2)	0.026(6)	0.05(1)	0.012(5)	0.04(1)
O_A8	0.14(2)	0.023(6)	0.023(6)	−0.040(9)	−0.021(8)	0.012(5)
O_A9	0.062(8)	0.033(7)	0.010(4)	0.028(7)	0.003(5)	0.004(5)
O_A10	0.059(8)	0.049(8)	0.01510*	−0.038(7)	0.007(5)	−0.005(5)
O_A11	0.11(1)	0.025(7)	0.019(7)	0.008(6)	0.032(8)	−0.004(5)
O_A12	0.053(8)	0.08(1)	0.008(4)	−0.036(9)	0.008(5)	−0.012(6)
O_A13	0.043(8)	0.037(6)	0.01500*	−0.013(6)	0.007(5)	0.000(5)
O_A14	0.030(6)	0.14(2)	0.024(6)	−0.045(9)	−0.007(5)	0.024(8)
O_B1	0.024(6)	0.029(5)	0.01500*	−0.002(5)	−0.002(4)	−0.001(4)
O_B2	0.023(5)	0.030(6)	0.009(4)	0.005(5)	0.008(3)	−0.003(4)
O_B3	0.072(9)	0.025(6)	0.008(4)	0.025(7)	0.009(5)	0.004(5)
O_B4	0.09(1)	0.019(7)	0.025(6)	0.017(6)	0.029(8)	0.009(5)
O_B5	0.07(1)	0.07(1)	0.01500*	−0.05(1)	0.001(6)	0.002(7)
O_B6	0.020(6)	0.053(8)	0.009(4)	0.011(5)	−0.002(4)	−0.015(5)
O_B7	0.030(7)	0.13(2)	0.011(5)	0.043(9)	0.004(4)	0.012(7)

Note: Starred parameters are fixed, standard deviations in parentheses, displacement parameters are of the form $\exp[-2\pi^2(U_{11}h^2a^{*2} + U_{22}k^2b^{*2} + U_{33}l^2c^{*2} + 2U_{12}hka^*b^* + 2U_{13}hla^*c^* + 2U_{23}klb^*c^*)]$.

rings [Schläfli symbol: $(6.5^2.4)\,(6.5^2)\,(6.5.4)$]. $Ba_2CuSi_2O_7$ (Malinovskii, 1984) and $KHoCoSi_2O_7$ (Ragimov et al., 1980) have the same stoichiometry as melilite types and possesses a two-dimensional $T1Si_2O_7$ network (T1 = Cu,Co) forming four- and six-membered rings [Schläfli symbol: $(6^2.4^2)\,(6^2.4)_2$] with Ba or K and Ho linking the layers.

Bond-strength calculations for layer topologies with $(T_3O_7)^{4+}$ composition

For all bond-strength calculations (Table 13) the empirical constants of Brown (1981) were used. Bond valences determined from experimentally determined bond lengths are used to calculate atomic valences, which can be used to evaluate a crystal structure. On the other hand, prediction of bond lengths is possible. Such calculations predict that eight-coordinate Ca should have average Ca-O distances (⟨Ca-O⟩) of approximately 2.45 Å. Kimata and Ohashi (1982) compared the Ca-O distances of gugiaite ($Ca_2BeSi_2O_7$) with those of melilite ($[Ca,Na]_2[Mg,Fe,AlSi]_3O_7$), hardystonite ($Ca_2ZnSi_2O_7$), gehlenite ($Ca_2Al_2SiO_7$), and akermanite ($Ca_2MgSi_2O_7$) and noticed that in gugiaite ⟨Ca-O⟩ = 2.521 Å, whereas in all other melilite-type structures ⟨Ca-O⟩ > 2.56 Å. In addition, Röthlisberger (1989) stated that in room-temperature electron diffraction experiments all known melilites of the type $Ca_2T1Si_2O_7$, except gugiaite ($Ca_2BeSi_2O_7$) with the smallest cation on T1 (Be), show satellite reflections indicating incommensurate structures. According to Röthlisberger (1989), no satellite reflections could be observed in melilite structures of the type $Sr_2T1Si_2O_7$ (T1 = Mg,Cu,Zn, Fe,Mn,Cd). Table 13 indicates that in all T_3O_7 sheet structures the X position (X = Ca,Sr,Ba) has low calculated valence values.

To estimate how well the T_3O_7 sheet structures fulfill a balanced electrostatic arrangement of atoms, a parameter $\Sigma|\delta|$ is calculated for all structures given in Table 13. The parameter $\Sigma|\delta|$ is the sum of magnitudes of the differences between the predicted and ideal atomic valences. Six atomic sites are distinguished: T1, T2, X, and the anions OI, OII, and OIII. (OI, OII, and OIII are equivalent to O1, O2, and O3 in melilite structures refined in space group $P\bar{4}2_1m$.) OI links two T2 tetrahedra, OII is only coordinated to T2 and X, and OIII links T1 and T2.

TABLE 8. Selected interatomic distances (Å) for the average low-$Ca_2ZnGe_2O_7$ structure

Zn_A1-O_A1	1.89(1)	Zn_A2-O_A5	1.94(2)
-O_A9	1.95(1)	-O_A7	1.93(2)
-O_A11	1.98(1)	-O_A8	1.98(1)
-O_A14	1.93(1)	-O_A3	1.98(1)
Ge_A3-O_A1	1.76(1)	Ge_A4-O_A7	1.74(1)
-O_A4	1.77(2)	-O_A10	1.78(1)
-O_A5	1.68(1)	-O_A11	1.74(1)
-O_A6	1.73(1)	-O_A12	1.72(1)
Ge_A5-O_A3	1.72(1)	Ge_A6-O_A2	1.71(1)
-O_A9	1.77(1)	-O_A4	1.76(2)
-O_A10	1.76(2)	-O_A8	1.75(1)
-O_A13	1.73(1)	-O_A14	1.72(1)
Zn_B1-O_B3	1.96(1)		
-O_B4	1.95(1)		
-O_B6	1.89(1)		
-O_B7	1.90(1)		
Ge_B2-O_B2	1.74(1)	Ge_B3-O_B1	1.72(1)
-O_B4	1.77(1)	-O_B3	1.74(1)
-O_B5	1.74(2)	-O_B5	1.80(2)
-O_B7	1.72(1)	-O_B6	1.75(1)
Ca_a1-O_A1	2.61(2)	Ca_a2-O_B4	2.46(2)
-O_A1	2.46(2)	-O_B5	2.99(2)
-O_A4	2.56(2)	-O_B8	2.48(2)
-O_A5	2.37(2)	-O_B12	2.63(1)
-O_A8	2.76(2)	-O_B13	2.75(1)
-O_A12	2.54(2)	-O_B13	2.48(1)
-O_A12	2.85(2)	-O_B14	2.74(2)
-O_A13	2.65(1)	-O_B14	2.42(2)
Ca_b1-O_A2	2.65(1)	Ca_b2-O_A6	2.43(1)
-O_A6	2.44(1)	-O_A7	3.21(2)
-O_A7	2.52(2)	-O_A9	2.54(1)
-O_A11	2.53(2)	-O_A10	2.51(1)
-O_B2	2.43(1)	-O_B1	2.54(1)
-O_B3	2.57(1)	-O_B2	2.52(1)
-O_B5	2.64(2)	-O_B4	2.46(2)
-O_B7	2.94(2)	-O_B7	2.57(2)
Ca_b3-O_A2	2.65(2)		
-O_A3	2.29(2)		
-O_A10	2.61(2)		
-O_B1	2.75(2)		
-O_B5	2.55(2)		
-O_B6	2.28(2)		
Ca_b4_a-O_A2	2.64(2)	Ca_b4_b-O_A2	3.16(6)
-O_A3	2.31(2)	-O_A3	2.14(5)
-O_A6	2.46(2)	-O_A6	2.30(4)
-O_A9	2.90(2)	-O_B1	2.61(4)
-O_B1	2.47(2)	-O_B3	2.50(6)
-O_B3	2.25(2)	-O_B4	2.13(4)
-O_B4	2.64(2)		
Ca_b5_a-O_A2	2.50(2)	Ca_b5_b-O_A2	2.45(5)
-O_A9	2.24(2)	-O_A9	2.48(8)
-O_A11	2.58(2)	-O_A11	2.04(6)
-O_B1	2.60(2)	-O_B1	3.22(9)
-O_B2	2.40(2)	-O_B2	2.40(5)
-O_B3	2.89(2)	-O_B6	2.13(7)
-O_B6	2.33(2)		

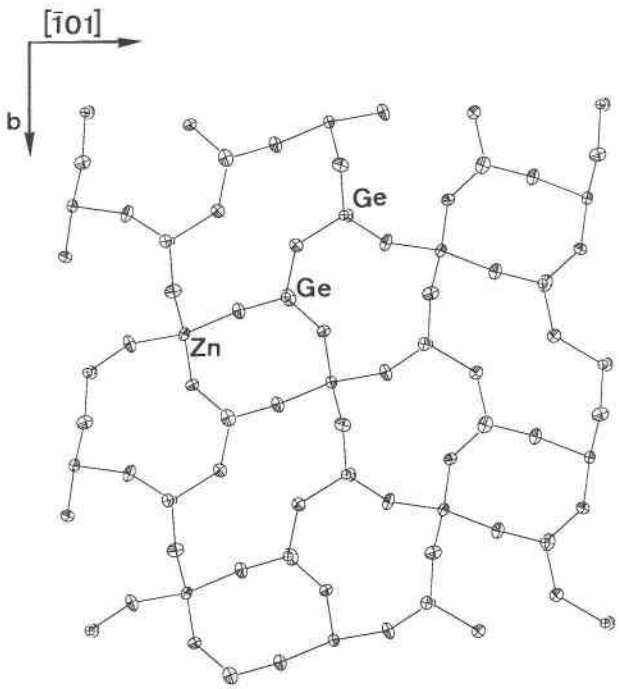

Fig. 6. ORTEP plot of the structure of $Ca_2ZnGe_{1.25}Si_{0.75}O_7$ (space group $P2_1/n$) viewed along [101]. Only a single tetrahedral layer (101) is shown. Compared to high and low $CaZnGe_2O_7$ (Figs. 2 and 4), the displacement ellipsoids of all atoms are much smaller and approximately isotropic, reflecting the nonmodulated character of this structure. (Scale of displacement ellipsoids is 70%.)

If owing to low symmetry one of these sites degenerates to two or more sites, average atomic valences are considered. Inspection of Table 13 reveals that the five structures with the highest $\Sigma|\delta|$ values are exactly those structures for which Röthlisberger (1989) observed satellite reflections. If there is a misfit between the size of the interlayer cation and the tetrahedral sheet, the layers become distorted, either in a disordered way, maintaining $P\bar{4}2_1m$ symmetry, or in an ordered fashion, adopting a modulated structure (Seifert et al., 1987). By solving an average crystal structure (without satellites), a difference between an ordered (modulated) and disordered fine structure cannot be resolved. As seen from the shape of anisotropic displacement ellipsoids (Fig. 2), the major effect of disorder or modulation in melilites is modeled as a rigid body libration of tetrahedral units around the *c* axis. This modeling has several effects on atomic coordinates and on atomic valences calculated from bond distances.

1. In a projection of the melilite structure along **c** (Fig. 2), the T2-O1-T2 link appears as a straight line, with O1 displaying strongly anisotropic displacements perpendicular to the T2-O1 vector. This indicates that in the fine structure the T2-O1-T2 angle is bent within (001), causing the real T2-O1 distance to be significantly longer than the apparent distance in the average structure.

2. It is also seen in Figure 2 that O1 and O3 displacement ellipsoids are elongated towards the center of the five-membered rings. Actually only O1 (constrained by symmetry) has its longest ellipsoidal axis in (001), 45° from *a*; the longest axis of the O3 displacement ellipsoids points towards the X site. These orientations indicate that the fine structure has significantly shorter X-O distances than the average model.

3. We assume that in the fine structure the T1 tetrahedron more or less maintains its $P\bar{4}$ symmetry, but it is disordered by a rigid body libration about $\bar{4}$ axis. This

TABLE 10. Population factors, coordinates, and equivalent isotropic displacement factors for $Ca_2ZnGe_{1.25}Si_{0.75}O_7$.

Atom	Pop.	x	y	z	B_{eq} (Å²)
Zn1	1.0	0.82867(3)	0.09678(3)	0.11477(3)	0.724(3)
Ge2	0.734(3) Ge 0.266 Si	0.87207(3)	0.45559(3)	0.20899(3)	0.481(3)
Ge3	0.521(3) Ge 0.479 Si	0.96891(4)	0.76878(4)	0.07667(4)	0.466(3)
Ca4	1.0	0.4574(1)	0.2821(1)	0.0282(1)	0.713(7)
Ca5	1.0	0.2891(1)	0.5654(1)	0.2014(1)	1.201(9)
O1	1.0	0.0094(2)	0.5682(2)	0.1572(2)	0.92(3)
O2	1.0	0.6321(2)	0.0625(2)	0.1343(2)	1.06(3)
O3	1.0	0.6915(2)	0.4557(2)	0.0501(2)	0.75(3)
O4	1.0	0.9672(2)	−0.0987(2)	0.2191(2)	0.74(3)
O5	1.0	0.8564(2)	0.1810(2)	−0.0651(2)	0.99(3)
O6	1.0	0.9545(2)	0.2625(2)	0.2764(2)	0.97(3)
O7	1.0	0.2959(2)	0.7292(2)	0.4207(2)	1.18(3)

Note: $B_{eq} = 8/3\ \pi^2\ \Sigma_i(\Sigma_j[U_{ij}\ a_i^*\ a_j^*\ a_i \cdot a_j)]$, $\sigma(B_{eq})$: Schomaker and Marsh (1983), standard deviations in parentheses.

effect causes shorter T1-O3 distances in the average model compared to the actual structure.

When we apply the above effects on bond-strength calculations, it becomes obvious that average models of modulated or statistically disordered melilites are characterized by apparent low valences for X sites (calculated X-O distances are too long), high valences for T1 and T2 positions (underestimation of T1-O and T2-O), and by overbonding of O1 because of the underestimated T2-O1 distance. On first glance it seems surprising that O3 shows no overbonding effects owing to underestimation of the distances T1-O3 and T2-O3 in average structures. However, the two X-O3 distances are both overestimated, which balances the calculated O3 valence. With the structural constraints of space group $P\bar{4}2_1m$ and a fairly rigid tetrahedral sheet, there is no degree of freedom to diminish simultaneously overbonding of O1 and to increase the bond strength on the X site.

The relation between calculated atomic valence, monitored in terms of the $\Sigma|\delta|$ parameter on one hand and the modulated or disordered character of an average melilite structure on the other, can even semiquantitatively be applied. For this purpose an additional parameter, Σdmax, is introduced, where dmax is the difference between the root mean square amplitude of the longest axis and the average value for the two shorter axes of a displacement ellipsoid (Table 14). Because disorder or modulation affects mainly O1 and O3, the parameter Σdmax is the sum of dmax values for O1 and O3; standard errors of Σdmax are large. Uncertainties in this value are related to the way in which main reflections accompanied by satellites are measured and how the data are refined. Figure 8 displays the relation between $\Sigma|\delta|$ and Σdmax. As expected, the four melilite-like crystals with a modulated fine structure (open squares in Fig. 8) display not only the highest $\Sigma|\delta|$ values but also the greatest anisotropies for the O1 and O3 displacement ellipsoids.

Grice and Hawthorne (1989) applied the same bond-valence model of Brown (1981) to leucophanite ($CaNaBeSi_2O_6F$) with space group $P2_12_12_1$ and obtained a more balanced bond-strength pattern than in any melilite-structure with space group $P\bar{4}2_1m$. The $\Sigma|\delta|$ value is 0.51. This low value can be explained by distortions in the tetrahedral layer and by the more variable chemical composition, both of which cause lower symmetry. In leucophanite, Si occupies one T1-type and one T2-type position. Be is ordered on an additional T2 site. One of the Si-Si bridging O atoms is additionally coordinated to two Na ions, and the other is coordinated to one Na and one Ca ion, thus reducing the overbonding. The apical

TABLE 11. Displacement parameters U_{ij} (Å²) for $Ca_2ZnGe_{1.25}Si_{0.75}O_7$

Atom	U_{11}	U_{22}	U_{33}	U_{12}	U_{13}	U_{23}
Zn1	0.0081(1)	0.0101(1)	0.0100(1)	0.0001(1)	0.0044(1)	0.0010(1)
Ge2	0.0061(1)	0.0061(1)	0.0061(1)	0.00000	0.00250	0.00000
Ge3	0.0059(1)	0.0059(1)	0.0059(1)	0.00000	0.00240	0.00000
Ca4	0.0087(2)	0.0107(2)	0.0071(2)	0.0024(2)	0.0026(2)	0.0006(2)
Ca5	0.0120(2)	0.0244(3)	0.0092(2)	0.0100(2)	0.0043(2)	0.0014(2)
O1	0.0102(8)	0.0115(8)	0.0137(8)	0.0009(6)	0.0053(7)	0.0024(7)
O2	0.0104(8)	0.0179(9)	0.0142(9)	0.0030(7)	0.0071(7)	0.0081(7)
O3	0.0086(7)	0.0112(8)	0.0084(8)	−0.0001(6)	0.0033(6)	0.0005(6)
O4	0.0116(8)	0.0085(8)	0.0077(7)	0.0016(6)	0.0035(6)	0.0001(6)
O5	0.0120(8)	0.0164(8)	0.0103(8)	0.0014(7)	0.0055(7)	0.0044(7)
O6	0.0145(9)	0.0117(8)	0.0073(8)	−0.0023(6)	0.0009(7)	−0.0005(6)
O7	0.0122(8)	0.0186(9)	0.0134(8)	−0.0010(7)	0.0047(7)	−0.0039(7)

Note: Standard deviations in parentheses, displacement parameters are of the form $\exp[-2\pi^2(U_{11}h^2a^{*2} + U_{22}k^2b^{*2} + U_{33}l^2c^{*2} + 2U_{12}hka^*b^* + 2U_{13}hla^*c^* + 2U_{23}klb^*c^*)]$.

TABLE 12. Selected interatomic distances (Å) for $Ca_2ZnGe_{1.25}Si_{0.75}O_7$

Zn1-O2	1.893(2)	Ge2-O1	1.757(2)	Ge3-O4	1.702(2)
-O4	1.893(2)	-O2	1.709(2)	-O1	1.729(2)
-O5	1.924(2)	-O3	1.712(2)	-O5	1.687(2)
-O6	1.977(2)	-O6	1.704(2)	-O7	1.658(2)
Ca4-O2	2.290(2)	Ca5-O1	2.410(2)		
-O3	2.421(2)	-O3	2.442(2)		
-O3′	2.473(2)	-O4	2.412(2)		
-O4	2.377(2)	-O5	2.805(2)		
-O6	2.378(2)	-O5′	2.455(2)		
-O7	2.575(2)	-O6	2.744(2)		
		-O7	2.871(2)		
		-O7′	2.410(2)		

Note: Standard deviations in parentheses.

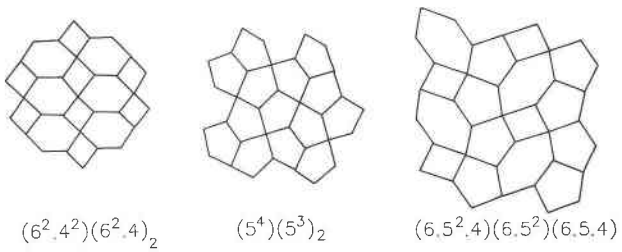

Fig. 7. Topologies of tetrahedral layers. The center of each tetrahedron is represented by a node, and the nodes are connected to form a two-dimensional network of polygons. From **left** to **right**: $Ba_2CuSi_2O_7$ type, melilite type, new type with space group $P2_1/n$.

anions (type OII in Table 13) displaced toward the interlayers tend to be underbonded in melilite-type structures. Two crystallographic positions of this type are present in leucophanite, and one of them is occupied by F.

Comparison of the $\Sigma|\delta|$ values of the high and low $Ca_2ZnGe_2O_7$ phases shows that the average low-$Ca_2ZnGe_2O_7$ structure displays a more balanced structure than that of the high modification. Overbonding of OI (Table 13) is even less than that of melilite structure types, and the average bond strength of the four fully occupied Ca sites is higher than in the average structure of high $Ca_2ZnGe_2O_7$.

TABLE 13. Bond strengths (valence units) on the basis of the empirical method of Brown (1981)

Compound	T2	T1	X	OI T2-T2	OII T2-X	OIII T1-T2	$\Sigma\|\delta\|$	Reference
$Ba_2CuSi_2O_7$	4.09	1.74	1.99	2.14	1.89	2.03	0.64	Malinovskii (1984)
						1.96		
			$P\bar{4}2_1m$ melilite-type compounds (only Si or Ge on T2)					
Ideal	4.0	2.0	2.0	2.0	2.0	2.0	0.00	
$Sr_2MgSi_2O_7$	4.16	1.93	1.84	2.40	1.76	2.00	1.03	Kimata (1983a)
$Sr_2MnSi_2O_7$	4.11	2.08	1.76	2.38	1.68	2.03	1.16	Kimata (1985)
$Ca_2BeSi_2O_7$	4.10	1.92	1.91	2.36	1.91	1.94	0.78	Kimata and Ohashi (1982)
$Ca_2MgSi_2O_7$*	4.04	2.06	1.65	2.38	1.65	2.01	1.19	Kimata and Ii (1981)
$Ca_2CoSi_2O_7$*	4.27	2.17	1.64	2.46	1.68	2.04	1.62	Kimata (1983b)
$Ca_2ZnSi_2O_7$*	4.15	2.13	1.68	2.38	1.70	2.00	1.28	Louisnathan (1969)
$Ca_2ZnGe_2O_7$*	4.38	2.04	1.59	2.49	1.79	1.98	1.55	This paper
$Sr_2ZnGe_2O_7$	3.92	1.96	1.67	2.32	1.72	1.90	1.15	Ochi et al. (1982)
$Ba_2FeGe_2O_7$	3.88	1.95	1.95	2.32	1.85	1.90	0.79	Malinovskii et al. (1976)
			$P\bar{4}2_1m$ melilite-type compounds (disordered Si and Al on T2)					
Ideal	3.5	3.0	2.0	2.0	2.0	2.0		
$Sr_2Al_2SiO_7$	3.54	2.96	1.86	2.23	1.79	1.97	0.69	Kimata (1984)
$Ca_2Al_2SiO_7$	3.53	3.04	1.75	2.26	1.62	2.01	0.97	Kimata and Ii (1982)
				Average low $Ca_2ZnGe_2O_7$*				This paper
	4.16	2.23	1.63	2.37	1.73	2.02		
	4.02	2.16	1.58	2.19	1.91	2.03		
	4.30	2.17	1.87	2.25	1.60	2.22		
	4.07		1.62		1.66	2.00		
			(1.70)		1.76	2.04		
			(1.78)		1.61	2.00		
			(1.45)			2.06		
			(1.87)			2.06		
			(2.03)			2.05		
						2.15		
						1.82		
						2.00	1.28	
				$P2_1/n$ $Ca_2Zn(Ge,Si)_2O_7$				This paper
	4.14	2.25	1.72	2.10	1.72	2.02		
	4.07		1.74			1.83		
						2.19		
						1.98		
						1.98	1.08	

Note: OI symbolizes an oxygen which links two T2 tetrahedra and is equivalent to O1 in melilite-type structures. OII symbolizes an oxygen vertex which is directed towards the interlayer cations (equivalent to O2 in melilite-type structures). OIII symbolizes an oxygen which links T1 and T2 tetrahedra and is equivalent to O3 in melilite-type structures. Bond strength values for partially occupied Ca sites are given in parentheses. $\Sigma|\delta|$ is the difference between the calculated and the ideal valence value summed over T2, T1, X, OI, OII, and OIII. If owing to lower symmetry more than one site is given, corresponding average values are taken for the summation.

* Satellite reflections.

The structure with space group $P2_1/n$ and the $(6.5^2.4)$ (6.5^2) (6.5.4) network has bond strengths that are approximately equal for all three types of O and the lowest $\Sigma|\delta|$ value of all of the phases with the general formula $Ca_2Zn(Ge,Si)_2O_7$. The displacement ellipsoids are approximately isotropic.

Stability relations of melilite-related compounds in the system CaO-ZnO-SiO_2-GeO_2

There are three possible explanations of how interlayer cations with various radii can be accommodated by the tetrahedral sheets: (1) preference of specific layer topologies as shown above, (2) variation in the stacking sequence of tetrahedral sheets, and (3) distortion within the tetrahedral sheets (lowering of symmetry and modulation).

The layer topologies $(6^2.4^2)$ $(6^2.4)_2$, (5^4) $(5^3)_2$ and $(6.5^2.4)$ (6.5^2) (6.5.4) have composition T_3A_7. Recent experiments by Röthlisberger (1989) indicate that a structure corresponding to that of $Ba_2CuSi_2O_7$ [that has a $(6^2.4^2)$ $(6^2.4)_2$ sheet] is not stable in the system CaO-ZnO-SiO_2-GeO_2. Sinter experiments between 1320 and 1420 K yielded a phase having the composition $Ba_2ZnSi_2O_7$ and a powder pattern corresponding to that of $Ba_2CuSi_2O_7$. Thus we assumed that the network type $(6^2.4^2)$ $(6^2.4)_2$ provides the largest eight-coordinated sites among the three kinds of layers with composition T_3O_7. In $Ba_2CuSi_2O_7$ the mean Ba-O distance is 2.814 Å (Malinovskii, 1984), and in $KHoCoSi_2O_7$ average K-O distances are 2.886 and 2.873 Å and average Ho-O distances are 2.708 and 2.781 Å (Ragimov et al., 1980).

At high temperatures the melilite-type sheet (5^4) $(5^3)_2$ has the preferred topology for $Ca_2ZnGe_2O_7$ and $Ca_2ZnSi_2O_7$. However, if these structures occur metastably at room temperature, the probable strong dynamic disorder of Ca is frozen at minima which do not obey space group $P\bar{4}2_1m$ symmetry but adopt an incommensurate arrangement that is also adopted by the tetrahedral layers.

It is not clear whether the ABA'ABA' stacking variant (low $Ca_2ZnGe_2O_7$) of the (5^4) $(5^3)_2$ network is a stable modification. None of the sinter or hydrothermal experiments in the system CaO-ZnO-SiO_2-GeO_2 by Röthlisberger (1989) produced this phase. It was only grown epitaxially on high $Ca_2ZnGe_2O_7$ and with a flux method for which high $Ca_2ZnGe_2O_7$ may have been the phase primarily formed. Perhaps this stacking variant formed under conditions where the high phase was exposed to intense internal strain, but where the activation energy was not sufficient to cause rearrangement of tetrahedral units to those of the phase with space group $P2_1/n$ that has the $(6.5^2.4)$ (6.5^2) (6.5.4) network. Thus, for strain minimization a partly reconstructed (an A'A melilite fragment is maintained) new stacking variant of the (5^4) $(5^3)_2$ network was adopted. Only weak Ca-O bonds must be broken for such a reconstructive transformation. Weak satellite reflections, large and strongly anisotropic displacement pa-

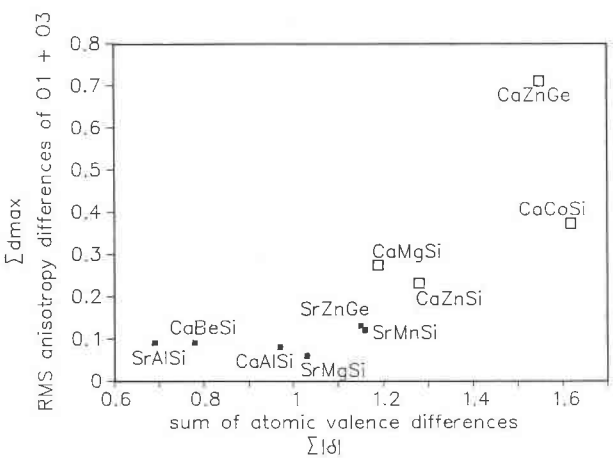

Fig. 8. The difference sum of calculated and ideal atomic valences ($\Sigma|\delta|$) is plotted versus an anisotropy parameter of O1 and O3 displacement ellipsoids of melilite structure types ($P\bar{4}2_1m$). Modulated structures represented by open squares have strong anisotropies for O1 and O3 in the average structures, resulting in an underestimation of T1-O and T2-O distances and thus affecting calculated atomic valences.

TABLE 14. Root-mean-square displacements (Å) along ellipsoid axes for O1 and O3 of melilite- and gehlenite-type structures

Compound Orientation	U1(O1) 45° a_1 45° a_2 90° c	U2(O1) −45° a_1 −45° a_2 90° c	U3(O1) 90° a_1 90° a_2 0° c	dmax O1	U1(O3) variable variable variable	U2(O3) variable variable variable	U3(O3) 25° a_1 110° a_2 75° c	dmax O3
$Sr_2MgSi_2O_7$	0.10	0.08	0.06	0.03	0.06	0.08	0.10	0.03
$Sr_2MnSi_2O_7$	0.14	0.10	0.09	0.04	0.06	0.08	0.15	0.08
$Ca_2BeSi_2O_7$	0.14	0.08	0.08	0.06	0.08	0.09	0.12	0.03
$Ca_2MgSi_2O_7$	0.27	0.14	0.09	0.15	0.10	0.12	0.23	0.12
$Ca_2CoSi_2O_7$	0.29	0.11	0.07	0.20	0.10	0.13	0.29	0.17
$Ca_2ZnSi_2O_7$	0.21	0.12	0.07	0.11	0.07	0.12	0.22	0.12
$Ca_2ZnGe_2O_7$	0.45	0.17	0.08	0.32	0.10	0.12	0.50	0.39
$Sr_2ZnGe_2O_7$	0.16	0.09	0.09	0.07	0.08	0.10	0.15	0.06
$Sr_2Al_2SiO_7$	0.12	0.07	0.09	0.04	0.07	0.09	0.13	0.05
$Ca_2Al_2SiO_7$	0.13	0.11	0.09	0.03	0.09	0.11	0.15	0.05

Note. dmax(O1) = U1 − (U2 + U3)/2, dmax(O3) = U3 − (U1 + U2)/2 orientations of ellipsoid axes labeled "variable" are different from compound to compound. For references consult Table 13.

rameters, and disordered Ca sites imply the modulated character of this stacking variant. The $(6.5^2.4)$ (6.5^2) (6.5.4) phase, which was grown at the lowest temperature, represents a well-ordered structure without any indication of modulations. Transformation from a (5^4) $(5^3)_2$ to a $(6.5^2.4)$ (6.5^2) (6.5.4) tetrahedral network must occur by a reconstructive mechanism.

The sequence of $Ca_2ZnGe_2O_7$ polymorphs with decreasing temperature thus is (5^4) $(5^3)_2$, $P42_1m$ (melilite-type structure), (5^4) $(5^3)_2$, $P2_1$ (stacking variant of the melilite structure), possibly metastable, and $(6.5^2.4)$ (6.5^2) (6.5.4), $P2_1/n$ (new structure type). The two (5^4) $(5^3)_2$ stacking variants may transform into modulated structures upon rapid cooling. Finally, it should be emphasized again that the $(6.5^2.4)$ (6.5^2) (6.5.4) layer structure is not the lock-in phase produced from a high-temperature phase with the melilite structure transforming through an incommensurately modulated structure into a commensurate superstructure; rather, it has an entirely different topology.

References cited

Bakakin, V.V., Belov, N.V., Borisov, S.V., and Soloveyva, L.P. (1970) The crystal structure of nordite and its relationship to melilite and datolite-gadolinite. American Mineralogist, 55, 1167–1181.

Brown, I.D. (1981) The bond valence method: An empirical approach to chemical structure and bonding. In M. O'Keeffe and A. Navrotsky, Eds., Structure and bonding in crystals II. Academic Press, New York.

Dal Negro, A., Rossi, G., and Ungaretti, L. (1967) The crystal structure of meliphanite. Acta Crystallographica, 23, 260–264.

Enraf Nonius (1983) Structure determination package (SDP). Enraf Nonius, Delft, The Netherlands.

Grice, J.D., and Hawthorne, F.C. (1989) Refinement of the crystal structure of leucophanite. Canadian Mineralogist, 27, 193–197.

Hemingway, B.S., Evans, H.T., Nord, G.L., Haselton, H.T., Robie, R.A., and McGee, J.J. (1985) Akermanite: Phase transitions in heat capacity and thermal expansion, and revised thermodynamic data. Canadian Mineralogist, 24, 425–434.

Kimata, M. (1983a) The structural properties of synthetic Sr-akermanite, $Sr_2MgSi_2O_7$. Zeitschrift für Kristallographie, 163, 295–304.

——— (1983b) The crystal structure and stability of Co-akermanite, $Ca_2CoSi_2O_7$, compared with the mineralogical behaviour of Mg cation. Neues Jahrbuch für Mineralogie Abhandlungen, 146, 221–241.

——— (1984) The structural properties of synthetic Sr-gehlenite, $Sr_2Al_2SiO_7$. Zeitschrift für Kristallographie, 167, 103–116.

——— (1985) The structural properties and mineralogical significance of synthetic $Sr_2MnSi_2O_7$ melilite with 4-coordinated manganese. Neues Jahrbuch für Mineralogie Monatshefte, 1985, 85–96.

Kimata, M., and Ii, N. (1981) The crystal structure of synthetic akermanite, $Ca_2MgSi_2O_7$. Neues Jahrbuch für Mineralogie Monatshefte, 1981, 1–10.

——— (1982) The structural properties of synthetic gehlenite, $Ca_2Al_2SiO_7$. Neues Jahrbuch für Mineralogie Abhandlungen, 143, 254–267.

Kimata, M., and Ohashi, H. (1982) The crystal structure of synthetic gugiaite, $Ca_2BeSi_2O_7$. Neues Jahrbuch für Mineralogie Abhandlungen, 143, 210–222.

Liebau, F. (1985) Structural chemistry of silicates: structure, bonding, and classification. Springer-Verlag, Berlin.

Louisnathan, S.J. (1969) The refinement of the crystal structure of hardystonite $Ca_2ZnSi_2O_7$. Zeitschrift für Kristallographie, 130, 427–437.

Malinovskii, Yu.A. (1984) Crystal structure of $Ba_2CuSi_2O_7$. Soviet Physics Doklady, 29, 706–708.

Malinovskii, Yu.A., Pobedimskaya, E.A., and Belov, N.V. (1976) Synthesis and X-ray analysis of two new iron-containing barium germanates $Ba_2FeGe_2O_7$ and $Fe_2NaBa_6Ge_8O_{24}\cdot 4(OH, H_2O)$. Kristallografiya, 21, 1195–1197.

Ochi, Y., Tanaka, K., Morikawa, H., and Marumo, F. (1982) The crystal structure of $Sr_2ZnGe_2O_7$. Kobutsugahu Zasshi (Journal of the Mineralogical Society of Japan), 15, 331–341.

Ragimov, K.G., Chiragov, M.I., and Mamedov, Kh.S. (1980) Crystal structure of the new synthetic silicate $KHoCoSi_2O_7$. Soviet Physics Doklady, 25, 583–584.

Röthlisberger, F. (1989) Zusammenhang zwischen Chemismus, Stabilität und struktureller Variation der Melilite. Ph.D. thesis, Universität Bayreuth, FRG.

Schomaker, V., and Marsh, R.E. (1983) On evaluating the standard deviation of U_{eq}. Acta Crystallographica, A39, 819–820.

Seifert, F., Czank, M., Simons, B., and Schmahl, W. (1987) A commensurate-incommensurate phase transition in iron-bearing akermanites. Physics and Chemistry of Minerals, 14, 26–35.

Sheldrick, G.M. (1976) SHELX76. Program for crystal structure determination. University of Cambridge, England.

——— (1986) SHELXS-86. Fortran-77 program for the solution of crystal structures from diffraction data. Institut für Anorganische Chemie der Universität Göttingen, FRG.

Smith, J.V. (1953) Reexamination of the crystal structure of melilite. American Mineralogist, 38, 643–661.

Zucker, U.H., Perenthaler, E., Kuhs, W.F., Bachmann, R., and Schulz, H. (1983) PROMETHEUS: A program system for investigation of anharmonic thermal vibrations in crystals. Journal of Applied Crystallography, 16. 358.

Manuscript received October 30, 1989
Manuscript accepted April 10, 1990